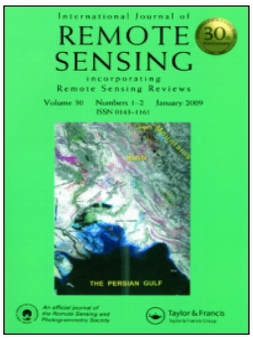

International Journal of Remote Sensing

ISSN: 0143-1161 (Print) 1366-5901 (Online) Journal homepage: www.tandfonline.com/journals/tres20

A UAV–lidar system to map Amazonian rainforest and its ancient landscape transformations

S. Khan, L. Aragão & J. Iriarte

To cite this article: S. Khan, L. Aragão & J. Iriarte (2017) A UAV–lidar system to map Amazonian rainforest and its ancient landscape transformations, International Journal of Remote Sensing, 38:8-10, 2313-2330, DOI: 10.1080/01431161.2017.1295486

To link to this article: https://doi.org/10.1080/01431161.2017.1295486

INTERNATIONAL JOURNAL OF REMOTE SENSING, 2017
VOL. 38, NOS. 8–10, 2313–2330
http://dx.doi.org/10.1080/01431161.2017.1295486

Taylor & Francis
Taylor & Francis Group

A UAV–lidar system to map Amazonian rainforest and its ancient landscape transformations

S. Khan[a], L. Aragão[b] and J. Iriarte[a]

[a]Department of Archaeology, University of Exeter, Exeter, UK; [b]Remote Sensing Division, National Institute for Space Research (INPE), São Jose dos Campos, Brazil

ABSTRACT

In this article, a robust unmanned aerial remote-sensing system, equipped with a survey-grade Lidar scanner and a multispectral camera system, assembled to study pre-Columbian Amazonian archaeology is presented. The data collected from this system will be utilized in a novel inter-disciplinary way by combining these data with *in situ* data collected by archaeologists, archaebotanists, paleoecologists, soil scientists, and landscape ecologists to study the nature and scale of the impact of pre-Columbian humans in transforming the landscapes of Amazonian rainforest. The outputs of this research will also inform future policy on the conservation, sustainability, and ecological state of the forest.

ARTICLE HISTORY
Received 31 July 2016
Accepted 9 February 2017

1. Introduction

Amazonia, the largest tropical rainforest of the world, plays a global role in regulating climate, sequestering carbon dioxide, and preserving biodiversity. Its protection and the development of sustainable land-use practices in Amazonia are of global significance (Lewis 2006; Bonan 2008). In order to make informed policy decisions on sustainable Amazonian futures, it is necessary to develop a sound understanding of the historical role of humans in shaping Amazonian landscapes and to what extent Amazonian forests were resilient to historical disturbances.

The nature and scale of pre-Columbian human impact in shaping Amazonian landscapes is a highly debated topic in New World archaeology, paleoecology and conservation. Until recently, the widely accepted concept was of a *noble-savage* who lived in harmony with the forest and had minimal impact on it (Ronnenberg, Bradshaw, and Marquet 2002; Meggers 1973; Steward 1963; Willey 1966). On the other hand, the opposite view hypothesizes the nonexistence of *virgin/natural* forest. It postulates that the rainforest was thriving with inhabitants distributed in social groups throughout the Amazon, who actively managed the forest, and extensively modified the ecosystems resulting in an anthropogenic and *domesticated landscape*. Recent archaeological studies propose that Amazonian landscape was transformed by sizeable, regionally-organized societies at a scale larger than previously suggested. This hypothesis is based on the discovery of domesticated landscape features like raised-field agriculture, highly

CONTACT S. Khan salman451@gmail.com Department of Archaeology, University of Exeter, Exeter, UK

modified anthropogenic soils called Amazonian Dark Earths (ADEs), hundreds of massive geometrically patterned earthworks called geoglyphs and ring-ditches, clusters of villages, well-planned mound complexes as well as the dominance of useful plant species in proximity of certain rivers (Denevan 2001; Balée and Erickson 2006; Schaan 2013; Rostain 2012; Levis et al. 2012), and is challenging the concept of Amazonia as a *virgin wilderness*. Many of these ancient landscape features have been revealed as a result of deforestation activities hinting that it is highly likely that many such features are still hidden under the forest waiting to be discovered (see Figure 1).

Traditionally, archaeological surveys have been done manually, but recently aerial remote sensing using high resolution lidar has been regarded as a more practical and cost-effective option. Further, environmental remote sensing using small unmanned aerial vehicles (UAVs) instead of manned aerial surveys has become a viable alternative (Whitehead et al. 2014). Unlike manual survey, airborne survey has the advantage of covering far greater area in a much shorter time and also the ability to record data over inaccessible remote regions of the Amazon rainforest. Lidar works on the same principle as Radar and Sonar: instead of using microwaves and sound waves, respectively, to calculate distance to a target, airborne lidar uses harmless laser pulses in infrared wavelengths to calculate the distance to the terrain below. Combining with ancillary data such as GPS measurements, aircraft attitude values, and lidar scan angles, etc. These terrain distances can be represented as a high resolution three-dimensional (3D) point cloud in World coordinates. In the context of Amazonian archaeology, the unique benefit of lidar manifests in its ability to penetrate through forest and reach the ground below. In this respect, lidar is often regarded as having the capability to see through vegetation, and can be used to identify previously unknown archaeological features (Prufer, Thompson, and Kennett 2015; Chase et al. 2011; Evans et al. 2013; Daukantas 2014). In practice, if there is a reasonably high density of lidar ground points, a 3D representation of the ground surface can be reproduced by connecting tiny planar surfaces representing neighbouring points, e.g. the triangulated irregular network (TIN) (Renslow, for Photogrammetry, and Sensing 2012). The resulting ground surfaces can be visually analysed in software tools by archaeologists and other experts to identify

Figure 1. Geoglyph partially revealed due to deforestation.

potential archaeological features, which can be later verified in ground survey. Moreover, lidar also facilitates studying the structure of forest from which very useful forest inventory metrics can then be derived. In this regard, the structure of forest over archaeological and non-archaeological sites can also be compared in order to understand ecological signatures of archaeological sites. Recently, the developments and improvements in small UAVs technology has also enabled the use of these lower cost platforms for producing very accurate and high resolution point cloud over forests (Wallace et al. 2012; Harwin and Lucieer 2012).

This article introduces a state-of-the-art unmanned aerial remote-sensing system assembled to document archaeology in Amazonian rainforest in order to assess the nature and scale of landscape transformations in Amazonia by pre-Columbian humans. It consists of a fixed-wing UAV, a survey-grade lidar scanner, and a low-cost 5-band camera system. The remainder of the article is organized as follows. Section 2 demonstrates the potential of lidar technology in studying Amazonian archaeology. Section 3 presents the unmanned aerial remote-sensing system including the UAV, its payloads, and the installation of the payloads in the UAV. Section 4 shows the first data collected using the remote-sensing system over different types of terrains. Section 5 proves that using the proposed remote-sensing system under forest features can be easily identified. Finally, Section 6 lists the conclusions and future plans of the research.

2. Potential of lidar in Amazonian archaeology

Considering a lidar scanner with a fixed laser wavelength and power, the density of ground points on a given area depends on the type of thickness of the vegetation, the measurement rate of the lidar scanner and the total data acquisition time.[1] The controllable factors are only the latter two. The higher the laser measurement rate and the longer the acquisition time the higher the density of the ground points for a given area. The minimum density of ground points required to identify an archaeological feature depends on its size. However, there is no strict rule of computing this minimum number and it can be more or less empirically determined.

In order to demonstrate the potential of using airborne lidar data to detect archaeology under the Amazon rainforest, a vegetation removal algorithm was applied to lidar data collected in Brazilian Amazon under the Sustainable Landscapes Brazil (Paisagens Sustentáveis Brasil) Project – SLBP. One such data, called the Bonal data, refers to the survey carried out in Rio Branco municipality, Acre state, Brazil. The Bonal data was acquired on 16 September 2013 using the Optech Orion laser scanner operating from an altitude of 900 m with a flight-line overlap of 65% covering a total area of 600 ha in 14 data tiles. The average point density was calculated to be approximately 33.39 points m^{-2}.

The application of vegetation removal algorithm on one tile of Bonal data is depicted in Figures 2(*a*)–(*c*). Figure 2(*a*) shows a Google Earth image of Bonal data tile demarked in yellow. The lidar data of the Bonal data tile, colour coded by height, are shown in Figure 2(*b*), while Figure 2(*c*) shows the ground surface formed by connecting the neighbouring ground points using a TIN after removing the non-ground/vegetation points. A close inspection of the ground surface reveals two rectangular features in close proximity to each other, marked by yellow circular boundaries. It is highly likely that these are geoglyphs, especially the larger, more prominent one, owing to the

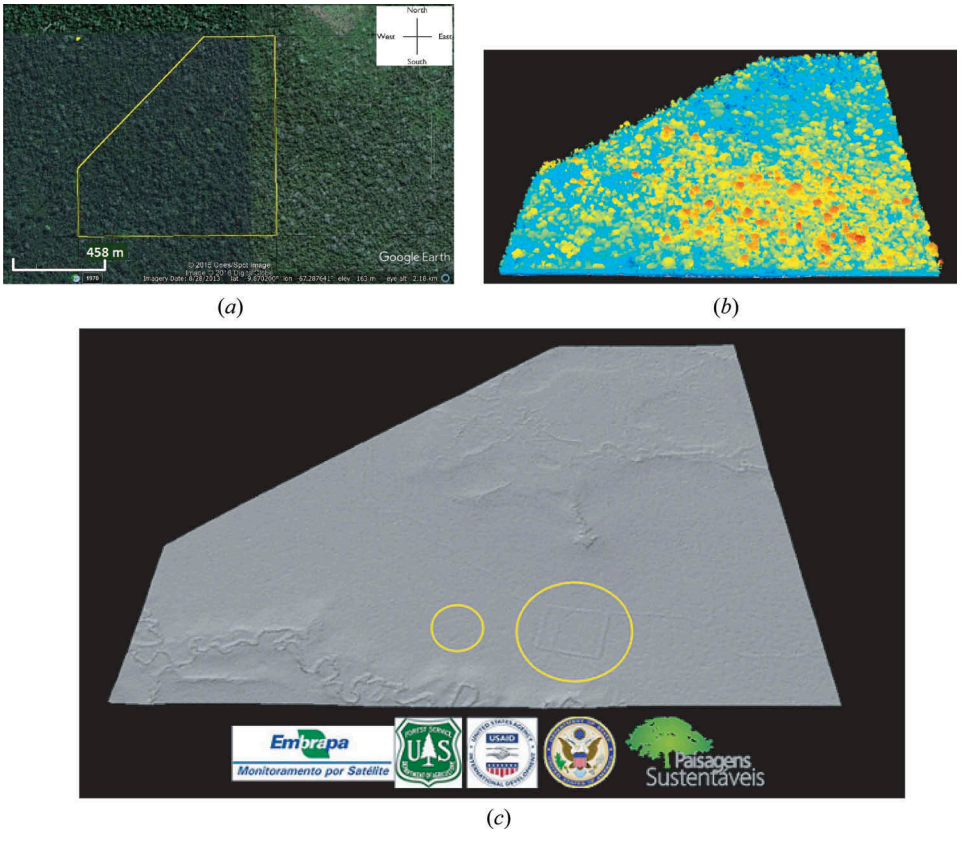

Figure 2. Airborne lidar data collected in Bonal, Rio Branco municipality, Acre, Brazil reveals under-forest geoglyphs. (*a*) A data tile from Bonal site – Google Earth image. (*b*) Colour-coded lidar data tile. (*c*) Vegetation removal algorithm reveals possible geoglyphs.

presence of many geoglyphs nearby exposed due to deforestation. However, this is yet to be confirmed by physically visiting these sites.

3. Remote-sensing system

The remote-sensing system consists of the NAURU 500B fixed wing UAV system fitted with the survey-grade VUX1–UAV lidar scanner and a 5-band camera system. The system is explained in more detail in the following sections.

3.1. *NAURU 500B fixed-wing UAV*

The NAURU 500B is a fixed-wing UAV developed by a Brazilian company, Xmobots. It is a fuel-run UAV with a 55cc two-stroke engine. It has a wing span of 3.6 m, a length of 1.8 m from nose to tail, and a maximum take-off weight of about 25 kg. It can carry approximately 5.5 kg of payload weight with an autonomy of around 2.5 h and has a stall speed of 31 knots. It requires a runway of about 80 m × 10 m for safe take-off and landing. NAURU has an autopilot system which can automatically execute a flight

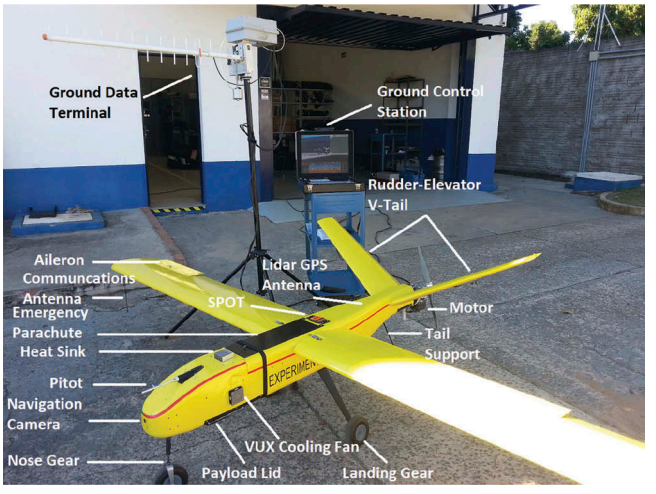

Figure 3. NAURU 500B fixed-wing UAV by Xmobots (wing span of 3.6 m and a nose to tail length of 1.8 m).

mission once the UAV has taken off manually. After completion of the mission, the UAV circles around the base station before it is manually landed by a remote control pilot. The UAV also includes a ground control station (GCS) and a ground data terminal (GDT) with an antenna that automatically tracks the aircraft. The GCS receives the flight telemetry, including the navigation

camera video, through the GDT to continuously monitor the mission, and also control the aircraft from a single user terminal. The NAURU 500B UAV, GCS, and GDT are shown in Figure 3, where various components of the system are appropriately labelled. The electronics of the aircraft are enclosed inside the fuselage where the heatsink is located. The electronic boards include the auto pilot and navigation board, router board, communications board, and VUX lidar connection board as shown in Figure 4.

3.2. *Payloads: VUX1–UAV lidar*

The VUX1–UAV by RIEGL is arguably the first survey-grade lidar scanner designed for UAV applications. It has a class 1, eye safe laser with a maximum effective measurement rate of 500,000 measurements/sec, a field of view of 330°, and a maximum operating flight altitude of 350 m. It is a light-weight and compact equipment weighing about 3.85 kg and measuring L 227 × W 180 × H 125 mm in dimensions without the cooling fans. It requires a voltage input of 11–32 V DC and typically 60 W power. Due to its high measurement rate it can produce a dense point cloud, e.g. at 380 kHz pulse repetition rate, flying at a speed of 50 knots, and a range to target of 250 m, the point density is approximately 10 points m^{-2} with a decimetre level accuracy. The point density can be further increased by increasing the percentage overlap between flight lines. The survey-grade APX-15 UAV INS/GNSS system by Applanix has been internally integrated into the VUX1–UAV scanner to reduce the positional errors to decimetre level. It is connected to the G5Ant-42AT1 L1/L2 GNSS antenna developed by Antcom. The GNSS antenna is fixed inside the NAURU airframe. The VUX1–UAV lidar scanner is shown in Figure 5(*a*). The

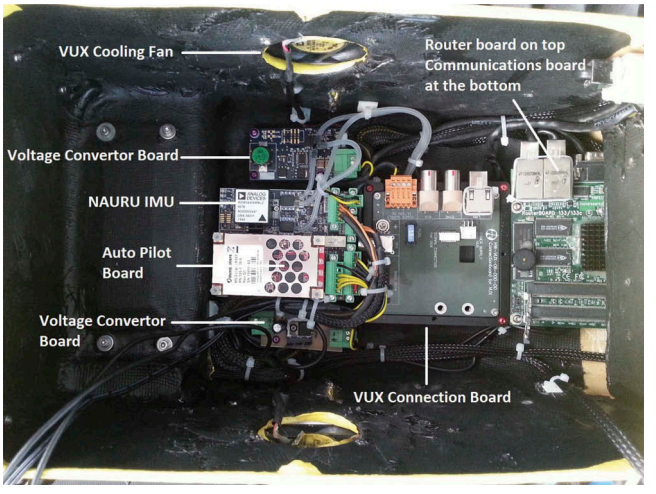

Figure 4. NAURU Electronics (width of the fuselage – top to bottom in the image – is about 19 cm).

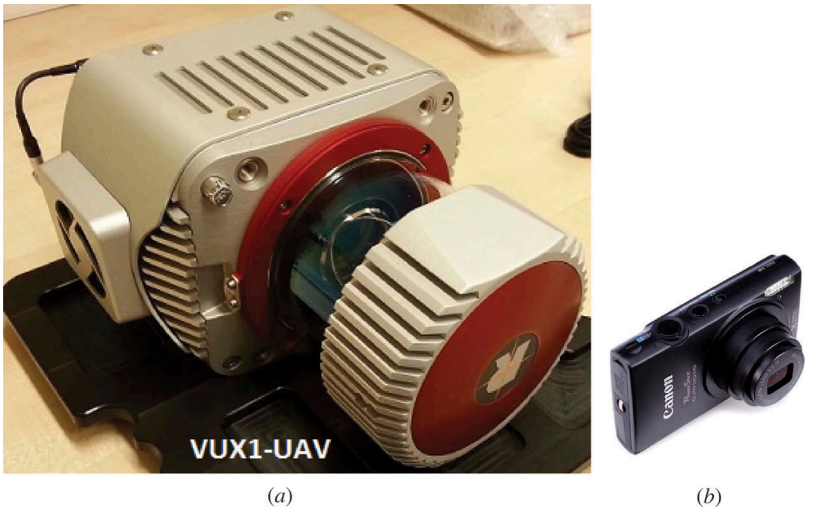

(*a*) (*b*)

Figure 5. Nauru payloads. (*a*) VUX1–UAV lidar scanner by RIEGL Laser Measurement Systems GmbH (dimensions without cooling fan – L 227 × W 180 × H 125 mm). (*b*) Canon PowerShot Elph110HS Camera (dimensions L 20.07 × W 93.22 × H 56.87 mm).

VUX1–UAV on-board NAURU is controlled using a workstation connected to the scanner through a wireless TCP/IP communication link provided by the GDT.

3.3. *Multispectral cameras*

Two low-cost multispectral Canon Powershot cameras (16 Megapixel) are also installed in the NAURU UAV. The dimensions of each camera are L 20.07 × W 93.22 × H 56.87 mm. Together they form a five-band multispectral system with one camera capturing in blue–green–near-infrared (NIR) 680–800 nm, while the other camera capturing in green–red–

NIR 800–900 nm. The camera settings are adjusted to suit aerial photography, e.g. the focus is set to infinity, shutter speed and aperture conditions are set for the conditions, etc. The cameras are installed in the fuselage of NAURU and are simultaneously triggered to take photos such that a pre-defined frontal overlap between adjacent photos is maintained. Similarly, the adjacent flight lines are also planned in such a way that the desired lateral overlap is achieved. Figure 5(*b*) shows one of the two identical multispectral cameras.

3.4. *Payload installation*

The two payloads of NAURU: VUX1 and cameras are securely screwed in NAURU's payload lid, which is then carefully inserted into the fuselage of NAURU from the bottom, and is subsequently secured in its place with 10 screws. Figures 6(*a*)–(*d*) show the installation of the payloads. Figures 6(*a*) and (*b*) depict the installation of the payloads in the payload lid from bottom and top perspectives, respectively. Figure 6 (*b*) also shows the aperture openings for the cameras and the VUX1 laser beam/glass protection lid which is controlled using a servo mechanism. During take-off and landing the servo closes the protection lid. Only during data acquisition the lid is kept open. Figure 6(*c*) presents the actual insertion of payload lid inside NAURU fuselage from the

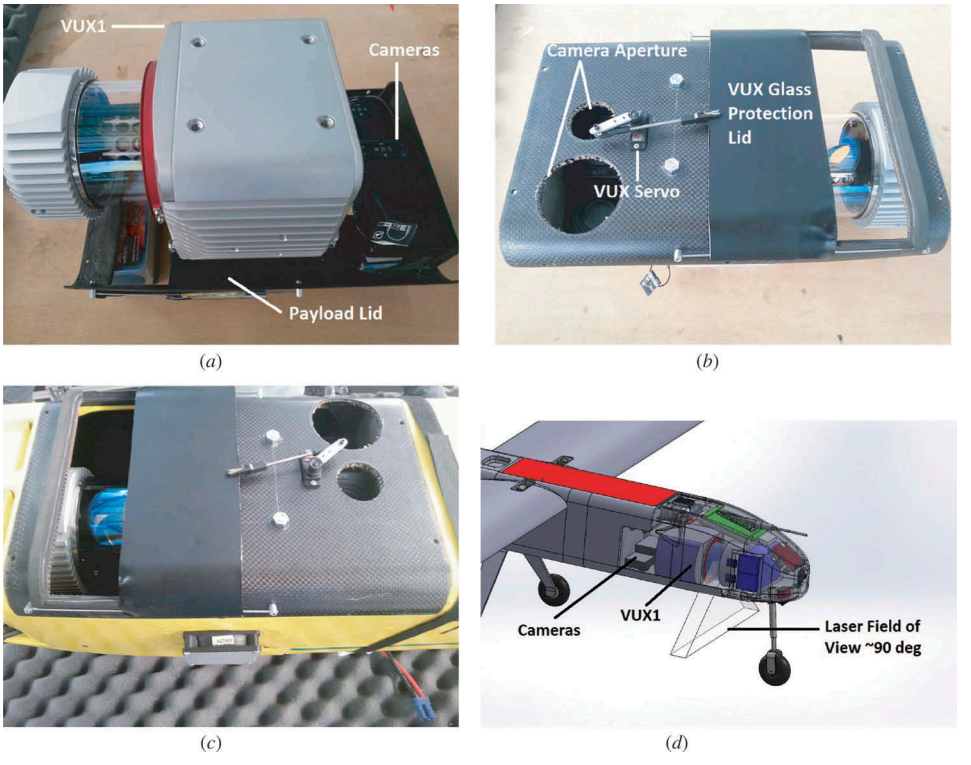

Figure 6. VUX1–UAV lidar scanner and cameras installed inside NAURU fuselage. (*a*) Installation of payloads in the lid (bottom view). (*b*) Installation of payloads in the lid (top view). (*c*) Insertion of payload lid in NAURU fuselage. (*d*) 3D CAD model of payload installation and field of view.

bottom, while Figure 6(*d*) shows the end result of the payload installation procedure in a 3D computer aided design (CAD) model diagram with the final location of the cameras and VUX1 inside NAURU. The laser field of view (FOV) is also shown in the figure, and has been measured to be approximately 90°. Two batteries of 6200 mAh each supply power to the system. One battery serves as the power source for NAURU's autopilot navigation system and the cameras while the other battery powers VUX1–lidar scanner.

4. Data acquisition campaigns

Lidar data collection using the NAURU-VUX lidar system was thoroughly tested in the last week of June, 2016. All flights were performed in a test area called Santana next to the city of São Carlos, SP, Brazil. Santana is primarily a sugar-cane agricultural area, but it also has forest patches and some gable-roof houses. Moreover, the runway is about 18 m wide and more than a 100 m long making it a well-suited test area. Four successful lidar data acquisition flights were carried out: one flight each on 24 and 27 of June, and two longer flights on the 29 June 2016. All different laser pulse repetition rates (PRR) of 50, 100, 200, 300, 380, and 550 kHz were tested at a flying altitude of 300 m above ground level (AGL). The lidar scan angles were restricted to 35° on either side of nadir, i.e. a total of 70°. Flying at 300 m AGL the ground swath is approximately 420 m. The aircraft flew at an average velocity of 58 knots (108 km h^{-1}). In order to maintain an even distribution of lidar points in along-track and across-track directions, the speed of the rotating laser mirror and the angular increment for sending laser pulses were adjusted accordingly. The weather conditions were very dry with clear skies, good visibility, and a wind speed ranging roughly between 4 and 10 knots.

The flights were planned using the Xmobot's flight planning software called *Mission Planning*. This software provides a satellite map based user interface to mark GPS waypoints over the area to be surveyed, and also allows the altitude of these waypoints to be adjusted. The first five waypoints are default ones, namely: (i) *Go_Home*, (ii) *Take-Off_1*, (iii) *Take-Off_2*, (iv) *Landing_1*, and (v) *Landing_2*. The *Go_Home* waypoint defines the GPS location at an altitude of 300 m AGL around which the UAV automatically circles before initiating (or after completing) an automatic mission. *Take-off_1* and *Take-off_2* represent the starting and ending points on the runway for the take-off procedures. While *Take-off_1* is located at the ground, *Take-off_2* is at an altitude of 20 m above ground. NAURU-500B UAV aircraft always takes-off manually controlled by a remote pilot, so the take-off waypoints are not used. The landing procedure, on the other hand, is manual under normal circumstances, however in case of a problem in remotely piloting the aircraft, the landing is performed by automatically opening the UAV's parachute. In this case, the UAV first circles around *Landing_1* while reducing its altitude to 100 m AGL. When the 100 m AGL is achieved, it goes to *Landing_2* and opens the parachute. The remaining waypoints are sequentially numbered, and are placed by the user such that the survey area is fully covered by lidar swath on the ground, with a user-selectable lateral overlap between adjacent flight lines to further increase lidar point density.

Figures 7(*a*) and (*b*) show the flight planning for a lidar mission collected on 29 June 2016 over an area in Santana, São Carlos, São Paulo state, Brazil. The area of interest was chosen to test the system in a variety of terrain and includes urban, agricultural, and forested regions as shown in Figure 7(*a*). The mission GPS waypoints are shown by blue

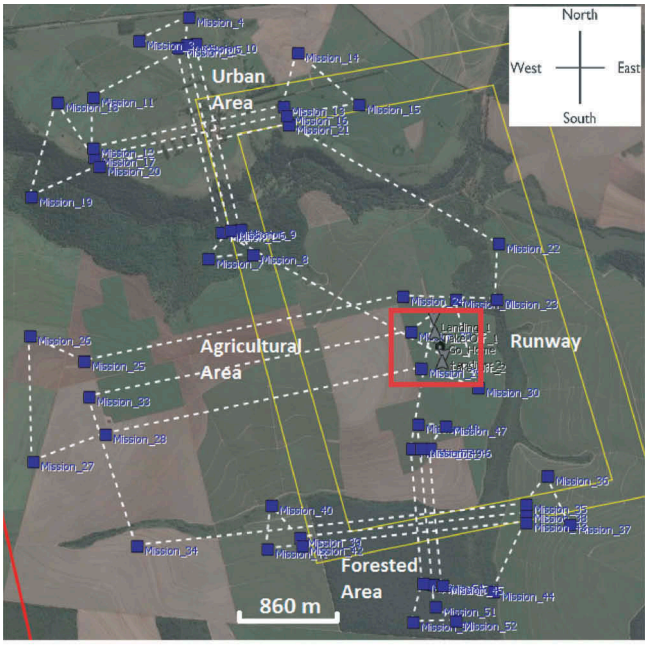

(*a*)

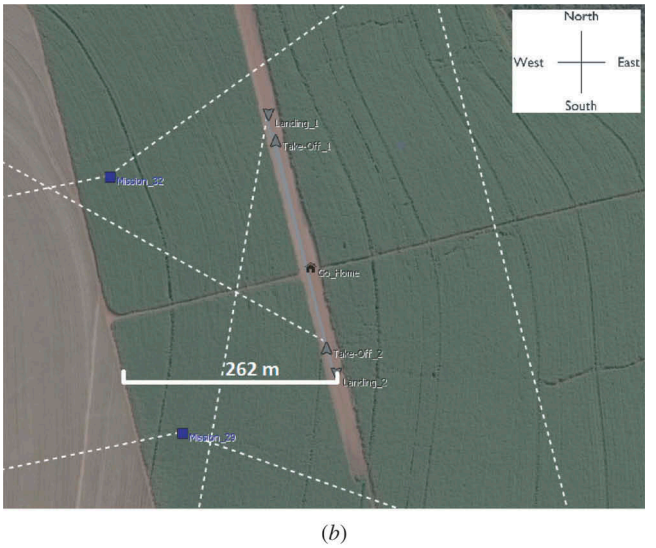

(*b*)

Figure 7. Nauru-500B UAV mission planning. (*a*) Mission plan for lidar data collected in Santana on 29 June 2016 over an area containing a mixture of urban, agricultural, and forested regions. (*b*) A zoomed-in view of the runway depicting the location of five default GPS waypoints.

squares, the flight lines by white dashed lines, while the five default waypoints have their distinct icons as shown in Figure 7(*b*). The real flight trajectory obtained from the actual position and orientation (POS) data is shown in Figure 8.

The flights are operated by first selecting a suitable space next to the runway where the GDT, GCS, and the UAV can be mounted. Ideally, the space should be free from

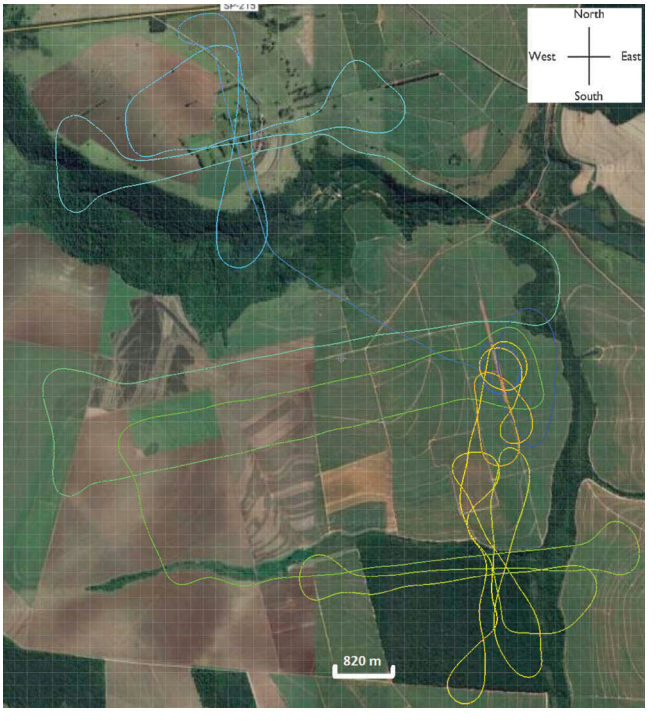

Figure 8. Real flight trajectory coloured by timestamp. Blue corresponds to start while red corresponds to end of the trajectory.

obstacles, safe, and at high vantage point. This is especially crucial for the seamless operation of the GDT, which transfers the UAV telemetry and navigation camera video to the GCS using the communication downlink. Once the equipment has been setup, a comprehensive checklist is followed to ensure that each part of the UAV and the supporting equipment (GCS and GDT) is correctly mounted and functioning appropriately. During this check, the intended flight mission is also uploaded into the aircraft's on board computer. After the successful completion of the checklist, the UAV's engine is started at which point the pilot is responsible for the take-off. After take-off the pilot flies the UAV to attain an altitude of 300 m AGL, while an operator at the GCS continuously monitors the real-time telemetric information and informs the pilot of the altitude and airspeed. Once the required altitude has been attained, the control of the UAV is passed to its autopilot. At this point, the UAV's mode of operation is *Go Home*, in which it circles around the *Go_Home* waypoint. The operator continuously monitors the telemetry while the UAV is in *Go Home* mode, and if all information is normal the operator starts the automatic mission after three circles around *Go_Home* waypoint. At this point, the remote pilot also switches off the remote control to conserve battery for landing. The UAV automatically follows the mission waypoints in sequence while the operator continuously monitors the telemetry to ensure that the UAV subsystems are operating perfectly. The lidar scanner is turned on and off by a separate operator who uses a notebook to control the VUX–1UAV lidar, while the communication between the notebook and the scanner is managed by the UAV's communication link. The operator starts

the laser at the start of each flight line and stops it at the end of the line. On mission completion, the GCS operator switches the UAV's mode of operation back to *Go Home*. During *Go Home* mode the UAV circles around the *Go_Home* point waiting for the pilot to assume back control of the aircraft for manual landing. After successful landing, the collected data is promptly downloaded for later processing before switching off all the systems.

In the following, we will present some sample lidar data collected in the aforementioned mission. The PRR was fixed at 300 kHz for this acquisition. The first study area, shown in Figures 9(*a*)–(*c*), is the urban area containing sparsely distributed trees, houses, and agricultural fields. Three of the total six flight lines over this area were planned in the horizontal direction, while the remaining three were roughly perpendicular to the first ones. The lateral overlap between consecutive flight lines was configured to be 80%. Figure 9(*a*) shows the 2D raster view (1 m^2 resolution) of the lidar data coloured by height. The trees, houses, and ground features are very clearly visible. Figure 9(*b*) shows 3D point cloud from one perspective with easily differentiable terrain features, while Figure 9(*c*) reveals the cross-sectional profile of a narrow area selected in Figure 9(*a*).

A little digression is necessary here to explain the misalignment in overlapping lidar strips. The boresight calibration models the rotational misalignment (in yaw, pitch, roll angles) and positional offset (in *X*, *Y*, *Z*) between the scanner and the IMU/GNSS system. The IMU/GNSS system describes the trajectory of the platform by measuring its GNSS location and its orientation in terms of the yaw, pitch, and roll angles. At the same time, the laser scanner detects the returning pulses at varying scan angles, and records the time that the pulses (traveling at the speed of light) take to travel from the scanner to the ground and back. The POS data, range to the ground, scan angles, and the boresight calibration parameters are then combined to determine the range vectors from the aircraft to ground points. Inherent systematic errors in any of these data usually lead to

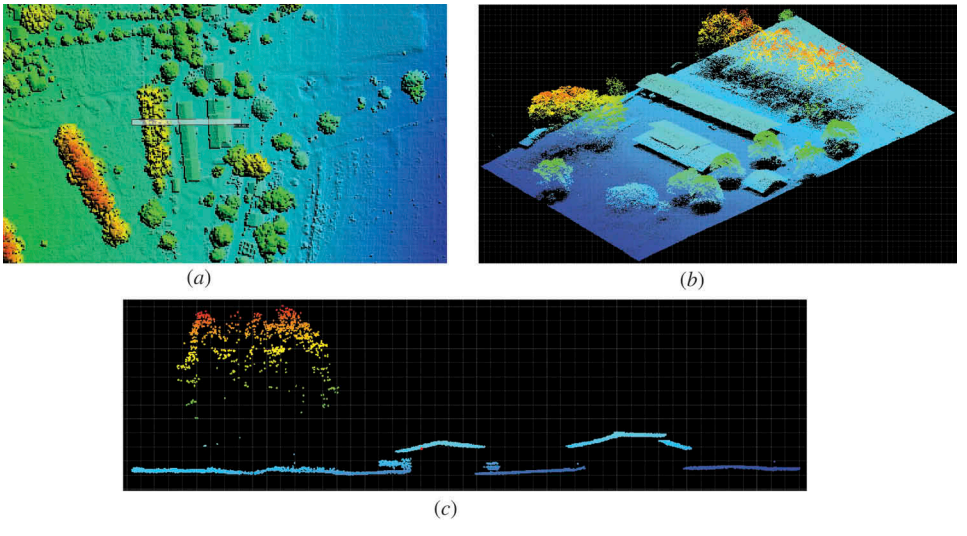

Figure 9. Lidar data (coloured by height) collected in Santana on 29 June 2016 over an area containing a mixture of houses, trees, and agricultural fields. (*a*) 2D-raster view of the data. (*b*) 3D view of a subset of the point cloud. (*c*) Cross-sectional profile of some houses and trees.

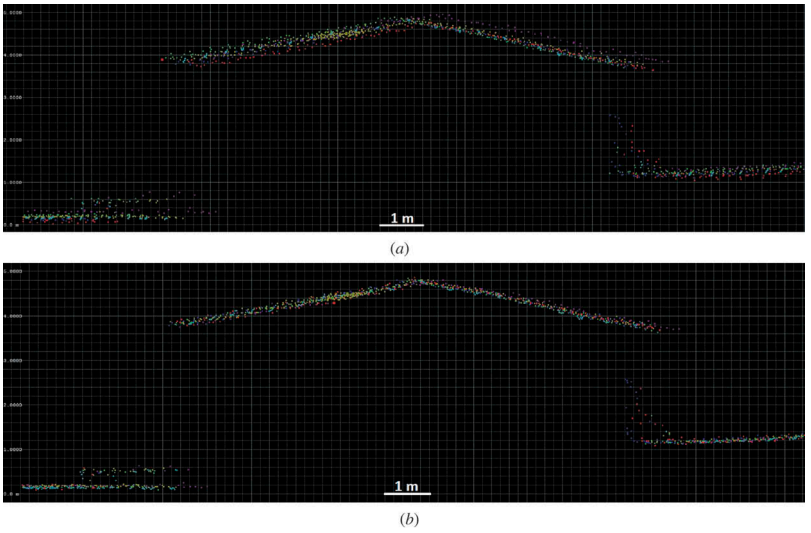

Figure 10. Scan data alignment after applying positional and rotational adjustments to trajectory data. (*a*) Misaligned lidar scans from separate flights lines. (*b*) Aligned lidar scans from separate flights lines after applying adjustment algorithm.

nonlinear rotational and positional errors between overlapping lidar strips (Habib et al. 2010; Glira, Pfeifer, and Mandlburger 2016). This can be easily observed in man-made structures and flat surfaces. Figure 10(*a*) shows the cross-sectional profile of a house with scan data from different flight lines shown in distinct colours. The scans from different flight lines are clearly misaligned from each other. Acknowledging the systematic errors of the lidar scanner and the IMU/GNSS system as inherent limitation of the hardware system, the remaining source of errors can be attributed to the inaccuracies (rotational and translational) in boresight calibration.

We have corrected the misalignment between overlapping strips by applying an algorithm which re-aligns the strips by modifying the original trajectory, i.e. the IMU/GNSS data. This algorithm is embedded as a routine called *RiPRECISION* within RIEGL's raw lidar data processing software, *RiPROCESS*. For brevity, we will present the error analysis only for the six overlapping strips over the urban area shown in Figure 7(*a*). The positional corrections to the trajectory, along-track, cross-track, and height are shown in Figure 11(*a*), while the orientation corrections in roll, pitch, and yaw angles of the trajectory are shown in Figure 11(*b*). The trajectory position corrections are negligible along- and cross-track, and only evident in height. This is evident in Table 1, which lists the statistics of positional corrections. The along- and cross-track corrections are sub-millimetre, while the height corrections are of the order of a few centimetres. Orientation corrections are less prominent in pitch and yaw and most visible in roll angles as also highlighted in Table 2, which shows the orientation correction statistics. The roll angle corrections are roughly an order of magnitude greater on the average. The corrected POS data can now be used to generate the revised point cloud, which shows an improved alignment of the overlapping strips. This is depicted in Figure 10(*b*), which visually shows that the lidar points from different lidar strips in the cross-sectional profile of the house are much better aligned together after applying the trajectory corrections.

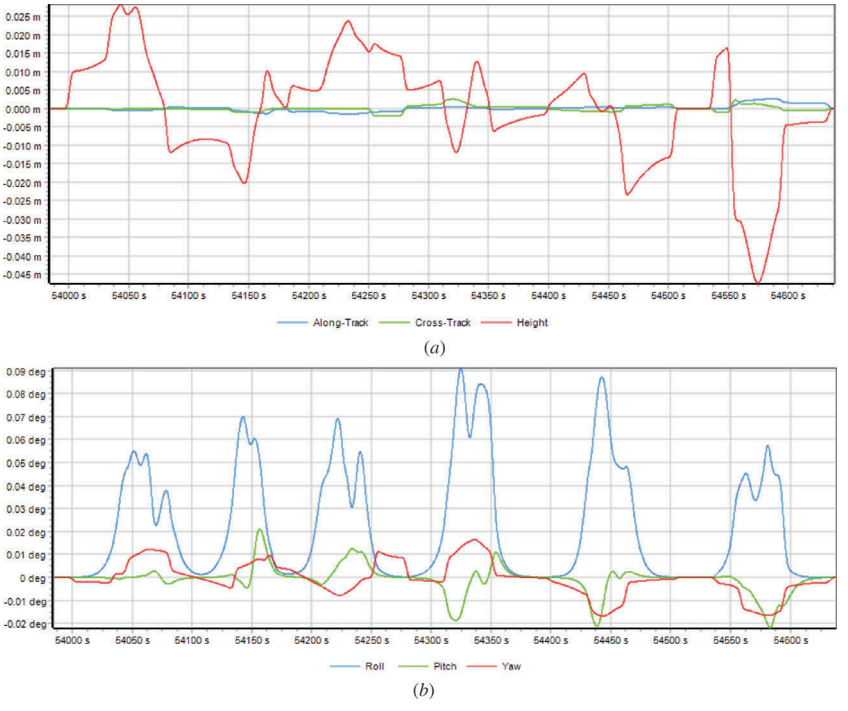

Figure 11. Trajectory corrections for six flight lines over urban area. (*a*) Trajectory positional corrections. (*b*) Trajectory orientational corrections.

Table 1. Statistics of positional corrections.

	Abs. mean (m)	Rms (m)	Max (m)
Along-track	0.0006	0.0009	0.0025
Cross-track	0.0006	0.0008	0.0025
Height	0.0113	0.0148	−0.0473
Total positional deviation	0.0114	0.0149	0.0474

Table 2. Statistics of orientation corrections.

	Abs. mean (deg)	Rms (deg)	Max (deg)
Roll angle	0.02325	0.03447	0.09099
Pitch angle	0.00335	0.00619	−0.02182
Yaw angle	0.00534	0.00733	−0.01673
Total angular deviation	0.02498	0.03578	0.09329

Let's return to presenting lidar data collected in the aforementioned mission. Figures 12(*a*)–(*c*) show the lidar data collected at 80% lateral overlap over the forested area with a total of six flight lines – three in horizontal and three in vertical direction. Figure 12(*a*) shows the 2D raster view of the forest lidar data coloured by height. The altitude in the lower-left corner of the raster is more (red) than that in the upper right corner (blue). Figure 12(*b*) shows a portion of the 3D forest point cloud, while Figure 12(*c*) displays the cross-sectional profile of a narrow selected forested area in Figure 12(*a*). It can be observed in Figures 12(*b*) and (*c*) that there are also a lot of ground points, shown in dark blue colour, under the forest.

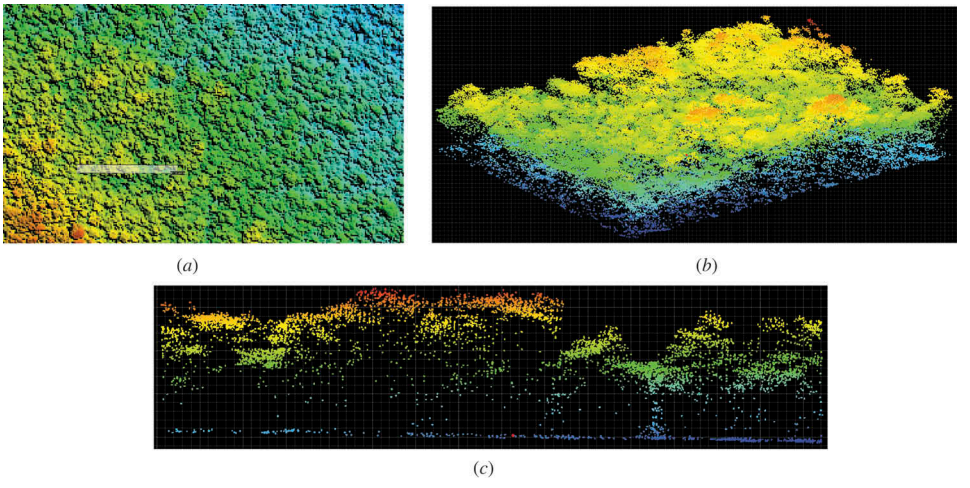

Figure 12. Lidar data (coloured by height) collected in Santana on 29 June 2016 over a forested area. (*a*) 2D-raster view of forested area. (*b*) 3D view of a subset of the forest point cloud. (*c*) Cross-sectional profile of a selected area.

Figure 13 shows a 2D raster view of some agricultural fields in Santana area. The boundaries of crops, ridges and other linear features are very easily visible in the figure. Moreover, three linear water storage mounds can also be identified in the centre, while a dirt road can be seen in the upper-left (blue) corner of the raster.

The images acquired from the multispectral cameras had the following issues: (1) they were not always properly focused despite setting the focus to infinity and disabling the auto-focus function, (2) the two cameras did not always trigger exactly at the same time with an average delay of about 20 ms resulting in additional processing to register the images between the two cameras. One solution to co-register the images from the two cameras is to first build the mosaic from the images from each camera and then use common features/markers between the mosaics to register them. The possible solutions to both of the above issues are currently under investigation. Figures 14(*a*)–(*c*) show

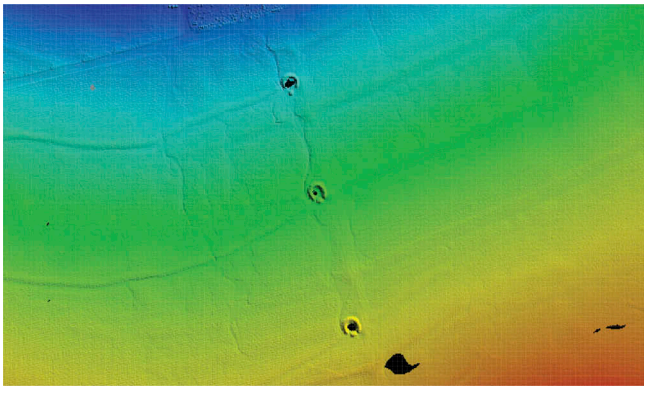

Figure 13. 2D-raster view of agricultural fields with easily identifiable patterns and three linear mounds for water storage.

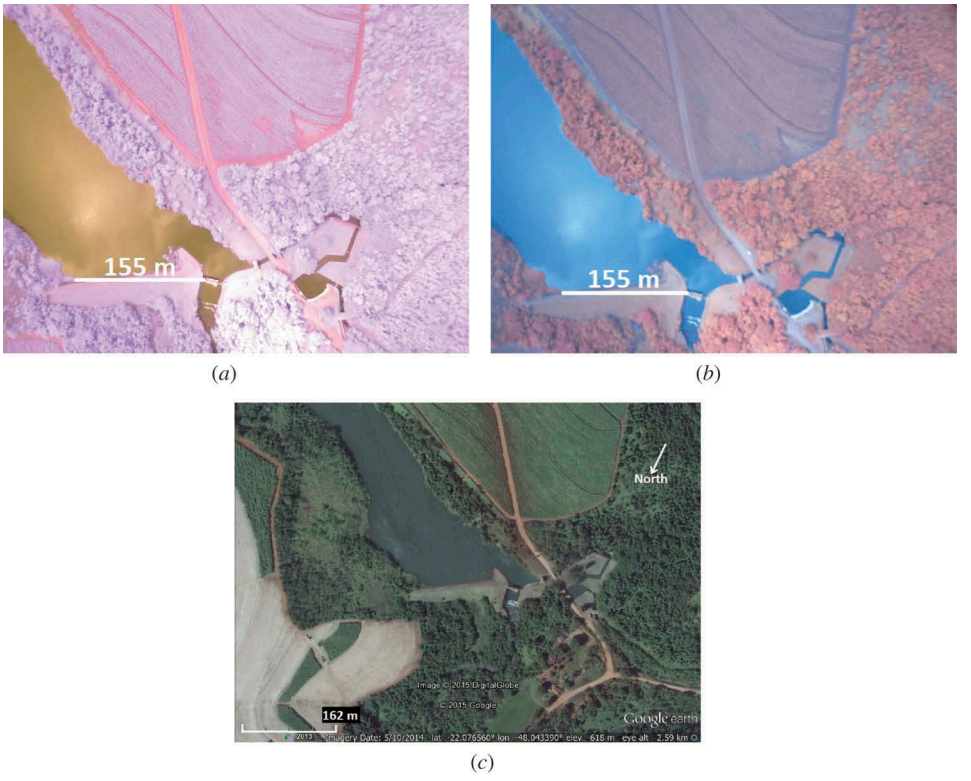

(*a*) (*b*) (*c*)

Figure 14. Sample photos from cameras. (*a*) Green–red–NIR 800–900 nm camera. (b) Blue–green–NIR 680–800nm camera. (*c*) Corresponding Google Earth Image.

sample images captured from the two cameras in a test mission. The upper-left corner coordinates are −22.076°, −48.042° while the lower-right ones are −22.075°, −48.048° (latitude, longitude).

5. Potential to discover under-forest features

The potential of airborne lidar to discover archaeological features under forest was demonstrated in Section 2 using data from SLBP. In this section, we will show that the lidar data collected using the NAURU/VUX UAV system also has this potential. In Figures 15(*a*)–(*d*), we have depicted forest removal algorithm applied on a few tiles of lidar data covering some forested and agricultural areas. The recording PRR was fixed at 300 kHz and the data is a collection of six overlapping flight lines with average point density of about 12 points m^{-2}. Figure 15(*d*) shows the tile boundaries of lidar data on a Google Earth optical image, while Figure 15(*a*) shows the 3D lidar point cloud of these tiles coloured by height. We used LASTools by rapidlasso GmbH to remove the forest point cloud and then connected the resulting ground points using TIN extrapolation to form the ground surface shown in Figure 15(*b*). The bulgy features along the top and bottom are artefacts of the triangulation process resulting due to the presence of insufficient lidar data and the misclassification of vegetation points as ground points. A close

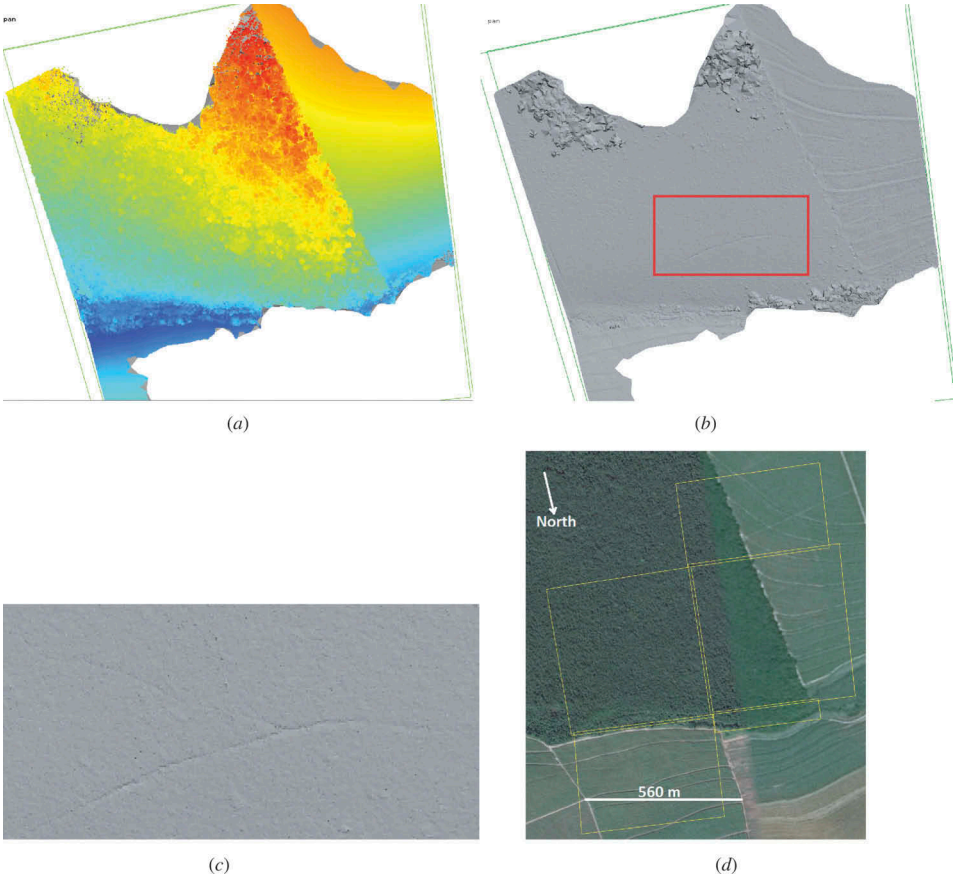

Figure 15. Lidar data collected at 300 kHz PRR in São Carlos, SP, Brazil reveals under-forest features. (*a*) Lidar point cloud colour-coded by height. (*b*) Vegetation removal reveals ground features. (*c*) Ground features easily visible when zoomed-in. (*d*) Corresponding data tiles – Google Earth image.

inspection of the ground surface in the red rectangle in Figure 15(*b*) reveals some linear features which could possibly be some pathway hidden underneath the forest. A zoomed-in version of the ground surface in the red rectangle is shown in Figure 15(*c*) where the under forest ground features are even more clearly visible. This shows that the lidar data collected through the proposed UAV/lidar system can be used to identify under forest features.

6. Conclusions and future work

Lidar technology has the potential to revolutionize archaeological survey in terms of time, resources, and cost. We have demonstrated that just like high-end airborne lidar systems our unmanned remote-sensing system is also capable of carrying out detailed lidar survey. The proposed system is not only able to study forest structure but also to re-create the ground surface below forests to identify archaeological sites and other hidden ground features. Visual analyses show that the collected lidar data are of acceptable quality for the

problem at hand. Moreover, it is quite straightforward to carry out data acquisition campaigns over forested areas as long as there is a reasonably sized runway available.

In the future, we need to find an effective solution to assure that the photos from the two cameras are focused and we also need to devise a workable method to register the photos from the two cameras together. Finally, we are planning to carry out our first set of data acquisition campaigns in Amazon rainforest in November, 2016.

Note

1. Data acquisition time also includes repeated passes over the same area.

Acknowledgements

The authors would like to thank European Research Council (ERC) for funding this research under the ERC Consolidator grant [616179] titled, *Pre-Columbian Amazon Scale Transformations*, and also express their gratitude to the Brazilian Agricultural Research Corporation (EMBRAPA), the US Forest Service, USAID, and the US Department of State for providing additional data.

Disclosure statement

No potential conflict of interest was reported by the authors.

Funding

This work was supported by the European Research Council [Pre-Columbian Amazon Scale Transformations].

References

Balée, W. L., and C. L. Erickson. 2006. *Time and Complexity in Historical Ecology: Studies in the Neotropical Lowlands*. The historical ecology series. New York: Columbia University Press.

Bonan, G. B. 2008. "Forests and Climate Change: Forcings, Feedbacks, and the Climate Benefits of Forests." *Science* 320 (5882): 1444–1449. doi:10.1126/science.1155121.

Chase, A. F., D. Z. Chase, J. F. Weishampel, J. B. Drake, R. L. Shrestha, K. Clint Slatton, J. J. Awe, and W. E. Carter. 2011. "Airborne Lidar, Archaeology, and the Ancient Maya Landscape at Caracol, Belize." *Journal of Archaeological Science* 38 (2): 387–398. doi:10.1016/j.jas.2010.09.018.

Daukantas, P. 2014. "Adding a New Dimension: Lidar and Archaeology." *Optics and Photonics News* 25 (1): 32–39. doi:10.1364/OPN.25.1.000032.

Denevan, W. M. 2001. *Cultivated Landscapes of Native Amazonia and the Andes. Oxford Geographical and Environmental Studies*. Oxford: Oxford University Press.

Evans, D. H., R. J. Fletcher, C. Pottier, J.-B. Chevance, D. Soutif, B. S. Tan, I. Sokrithy. et al. 2013. "Uncovering Archaeological Landscapes at Angkor Using Lidar." *Proceedings of the National Academy of Sciences* 110 (31): 12595–12600. doi:10.1073/pnas.1306539110.

Glira, P., N. Pfeifer, and G. Mandlburger. 2016. "Rigorous Strip Adjustment of UAV-Based Laserscanning Data Including Time-Dependent Correction of Trajectory Errors." *Photogrammetric Engineering and Remote Sensing* 82 (12): 945–954. doi:10.14358/PERS.82.12.945.

Habib, A., K. I. Bang, A. P. Kersting, and J. Chow. 2010. "Alternative Methodologies for Lidar System Calibration." *Remote Sensing* 2 (3): 874–907. doi:10.3390/rs2030874.

Harwin, S., and A. Lucieer. 2012. "Assessing the Accuracy of Georeferenced Point Clouds Produced via Multi-View Stereopsis from Unmanned Aerial Vehicle (UAV) Imagery." *Remote Sensing* 4 (6): 1573–1599. doi:10.3390/rs4061573.

Levis, C., P. F. De Souza, J. Schietti, T. Emilio, J. L. P. V. Pinto, C. R. Clement, and F. R. C. Costa. 2012. "Historical Human Footprint on Modern Tree Species Composition in the Purus-Madeira Interfluve, Central Amazonia." *PLoS One* 7: e48559. doi:10.1371/journal.pone.0048559.

Lewis, S. L. 2006. "Tropical Forests and the Changing Earth System." *Philosophical Transactions of the Royal Society of London B: Biological Sciences* 361 (1465): 195–210. doi:10.1098/rstb.2005.1711.

Meggers, B. J. 1973. *Amazonia: Man and Culture a Counterfeit Paradise*. Worlds of man. Chicago, IL: Aldine Publishing Company.

Prufer, K. M., A. E. Thompson, and D. J. Kennett. 2015. "Evaluating Airborne Lidar for Detecting Settlements and Modified Landscapes in Disturbed Tropical Environments at Uxbenká, Belize." *Journal of Archaeological Science* 57 (Complete): 1–13. doi:10.1016/j.jas.2015.02.013.

Renslow, M. S., American Society for Photogrammetry, and Remote Sensing. 2012. *Manual of Airborne Topographic Lidar*. Imaging & Geospatial Information Society.

Ronnenberg, K. L., G. A. Bradshaw, and P. Marquet. 2002. *How Landscapes Change: Human Disturbance and Ecosystem Fragmentation in the Americas*. Ecological Studies. Berlin/Heidelberg: Springer.

Rostain, S. 2012. "Between Sierra and Selva: Landscape Transformations in Upper Ecuadorian Amazonia." *Quaternary International* 249: 31–42. Long-term perspectives on human occupation of tropical rainforests. doi:10.1016/j.quaint.2011.08.031.

Schaan, D. P. 2013. *Sacred Geographies of Ancient Amazonia: Historical Ecology of Social Complexity*. New Frontiers in Historical Ecology. Walnut Creek, CA: Left Coast Press.

Steward, J. H. 1963. *Handbook of South American Indians*. New York: Cooper Square Publisher.

Wallace, L., A. Lucieer, C. Watson, and D. Turner. 2012. "Development of a UAV-Lidar System with Application to Forest Inventory." *Remote Sensing* 4 (6): 1519–1543. doi:10.3390/rs4061519.

Whitehead, K., C. H. Hugenholtz, S. Myshak, O. Brown, A. LeClair, A. Tamminga, T. E. Barchyn, B. Moorman, and B. Eaton. 2014. "Remote Sensing of the Environment with Small Unmanned Aircraft Systems (UASs), Part 2: Scientific and Commercial Applications." *Journal of Unmanned Vehicle Systems* 02 (03): 86–102. doi:10.1139/juvs-2014-0007.

Willey, G. R. 1966. *An Introduction to American Archaeology: South America*. Prentice-Hall anthropology series. Upper Saddle River, NJ: Prentice-Hall.